

# Crystal chemistry of Sr-rich piemontite from manganese ore deposit of the Tone mine, Nishisonogi Peninsula, Nagasaki, southwest Japan

Mariko NAGASHIMA\*, Yuko SANO\*\*, Takako KOCHI\*\*, Masahide AKASAKA\*\*\* and Asami SANO-FURUKAWA†

\*Division of Earth Science, Graduate School of Science and Technology for Innovation, Yamaguchi University, Yamaguchi 753-8512, Japan

\*\*Department of Geosphere Science, Faculty of Science, Yamaguchi University, Yamaguchi 753-8512, Japan

\*\*\*Department of Geoscience, Interdisciplinary Graduate School of Science and Engineering, Shimane University, Matsue 690-8504, Japan

†J-PARC Center, Japan Atomic Energy Agency, Tokai-mura, Ibaraki 319-1195, Japan

The crystal chemistry of Sr-rich piemontite from a layered manganese ore deposit of the Tone mine, Nishisonogi Peninsula, Japan, was studied using methods of electron microprobe analysis, single crystal X-ray structural refinement,  $^{57}\text{Fe}$  Mössbauer spectroscopy, and X-ray and Time-of-Flight neutron Rietveld analyses to elucidate the intracrystalline distributions of Sr, Mn, and Fe and the general and individual features on the structural changes with Sr contents in piemontite and epidotes. Piemontite in the most piemontite-dominant layer of an ore is  $[\text{Ca}_{1.73(15)}\text{Sr}_{0.22(13)}]_{\Sigma 1.95}[\text{Al}_{1.99(9)}\text{Mn}_{0.68(8)}^{3+}\text{Fe}_{0.37(8)}^{3+}\text{Mg}_{0.01(0)}]_{\Sigma 3.05}\text{Si}_{2.99(1)}\text{O}_{12}(\text{OH})$  ( $Z = 2$ ) in the average chemical formula. A single crystal X-ray structural refinement ( $R_1 = 2.51\%$  for 2417 unique reflections) resulted in the unit-cell parameters of  $a = 8.8942(1)$ ,  $b = 5.6540(1)$ ,  $c = 10.1928(2)$  Å, and  $\beta = 115.100(1)^\circ$ ; and the occupancies of  $\text{Ca}_{0.711(3)}\text{Sr}_{0.289}$ ,  $\text{Al}_{0.898(4)}(\text{Mn} + \text{Fe})_{0.102}$ , and  $(\text{Mn} + \text{Fe})_{0.949(4)}\text{Al}_{0.051}$  at the  $^{\text{X}}\text{A}2$ ,  $^{\text{VI}}\text{M}1$ , and  $^{\text{VI}}\text{M}3$  sites, respectively. All Fe in a powdered piemontite sample was  $\text{Fe}^{3+}$  as indicated by the two Mössbauer doublets (isomer shift = 0.351 and 0.367 mm/s and quadrupole splitting = 2.189 and 1.93 mm/s, respectively) assigned to  $\text{Fe}^{3+}$  at the  $\text{M}3$  site. The neutron Rietveld refinement of the powder sample ( $R_{\text{wp}} = 2.11\%$ ;  $R_e = 0.88\%$ ) resulted in the occupancies of  $^{\text{M}1}[\text{Al}_{0.902(5)}\text{Mn}_{0.098}]$  and  $^{\text{M}3}[\text{Mn}_{0.534(5)}\text{Fe}_{0.267}\text{Al}_{0.20}]$ , where  $^{\text{M}3}\text{Al}$  was fixed to 0.20Al obtained by X-ray Rietveld refinement ( $R_{\text{wp}} = 2.95\%$ ;  $R_e = 2.13\%$ ). By applying the oxidation state of Fe and the distributions of Al, Fe, and Mn in the  $\text{M}1$  and  $\text{M}3$  sites in the powder sample, the site occupancies in the piemontite single crystal are constructed as  $^{\text{A}2}[\text{Ca}_{0.711(3)}\text{Sr}_{0.289}]$ ,  $^{\text{M}1}[\text{Al}_{0.898(4)}\text{Mn}_{0.102}^{3+}]$  and  $^{\text{M}3}[\text{Mn}_{0.633}^{3+}\text{Fe}_{0.316}^{3+}\text{Al}_{0.051}]$ . The  $\text{A}2\text{-O}7$ ,  $\text{-O}2'$ , and  $\text{-O}10$  distances, 2.303(2), 2.562(1), and 2.592(2) Å, respectively, are longer than those of Ca-piemontites. The mean  $\langle \text{M}3\text{-O} \rangle$  and  $\langle \text{M}1\text{-O} \rangle$  distances, 2.050 and 1.923 Å, respectively, are close to the published data of Ca-piemontites and Sr-rich and -bearing piemontites with  $\text{Mn}^{3+} + \text{Fe}^{3+}$  contents in the  $\text{M}3$  and  $\text{M}1$  sites similar to those of the Tone piemontite.

**Keywords:** Strontian Piemontite, Tone mine, X-ray diffraction, TOF neutron diffraction, Mössbauer analysis, Crystal structure

## INTRODUCTION

Epidote-supergroup minerals are monoclinic in symmetry and have space group  $P2_1/m$  and the structural formula of  $\text{A}2\text{A}1\text{M}1\text{M}2\text{M}3[\text{T}_2\text{O}_7][[\text{TO}_4](\text{O},\text{F})(\text{OH},\text{O})]$ , where  $\text{A}2$  and  $\text{A}1$  imply 10-coordinated and 9-coordinated sites, respectively;  $\text{M}1$ ,  $\text{M}2$ , and  $\text{M}3$  represent octahedral sites;

and  $\text{T}$  is tetrahedral sites (Armbruster et al. 2002; Mills et al., 2009). Epidote-group minerals of epidote-supergroup, such as clinozoisite, epidote and piemontite, are important Sr containers in metamorphic rocks (e.g., Grapes and Watanabe, 1984; Mottana, 1986; Reinecke, 1986; Nagasaki and Enami, 1998; Enami, 1999; Miyajima et al., 2003; Nagashima et al., 2006), metamorphosed manganese ore deposits (e.g., Kato and Matsubara, 1986; Bonazzi et al., 1990; Perseil, 1990; Minakawa, 1992; Nagashima et al., 2007; Minakawa et al., 2008; Nagashima et

doi:10.2465/jmps.191122

M. Nagashima, nagashim@yamaguchi-u.ac.jp Corresponding author

al., 2010), and metamorphosed manganiferous iron ore deposits (Akasaka et al., 1988; Togari et al., 1988). Thus, the occurrence and crystal chemical properties of Sr-bearing epidote-group minerals, such as solubility of Sr and its effect on the Mn and Fe contents and crystal structure, have been interested in.

The Sr contents of epidote-group minerals in the published studies cited above are less than 1 atom per formula unit (apfu). According to Akasaka et al. (2000), the synthetic piemontite in the join  $\text{Ca}_2\text{Al}_2\text{Mn}^{3+}\text{Si}_3\text{O}_{12}(\text{OH})$ - $\text{Sr}_2\text{Al}_2\text{Mn}^{3+}\text{Si}_3\text{O}_{12}(\text{OH})$  also contained Sr up to 1 apfu. Such results are consistent with those clarified by the X-ray structural refinements that  $\text{Sr}^{2+}$  ions occupy only the larger 10-coordinated *A2* site but not the smaller 9-coordinated *A1* site in the epidote structure (Bonazzi et al., 1990; Armbruster et al., 2002; Miyajima et al., 2003; Nagashima et al., 2010). Dörsam et al. (2007) indicated that the synthetic clinozoisite  $(\text{Ca}, \text{Sr})_2\text{Al}_3\text{Si}_3\text{O}_{12}(\text{OH})$  having Sr occupancy of  $>0.8$  at the *A2* site simultaneously contains Sr reaching up to 0.15(4) in occupancy at the *A1* site. However, it is not the case of natural Sr-rich piemontite, as typically shown by strontioepimontite in which the *A2* site is occupied by 0.68 Sr (Bonazzi et al., 1990) and tweddillite with Sr occupying fully the *A2* site (Armbruster et al., 2002). Whereas the smaller 9-coordinated *A1* site is occupied by Ca and additional  $\text{Mn}^{2+}$ , as clarified by the structural studies by Armbruster et al. (2002) and Nagashima et al. (2010).

In order to elucidate the general and individual features on the structural changes with Sr contents in epidotes, characterization of the epidote-group minerals containing various amounts of Sr has been required. With regard to Sr-rich piemontite, in addition to the maximum contents of Sr and transition metal ions and to the structural change due to the incorporation of Sr in the *A2* site, the variation in intracrystalline partitioning of transition metal ions accompanying with the substitution of Sr for Ca have been particularly concerned (e.g., Ferraris et al., 1989; Bonazzi et al., 1990; Armbruster et al., 2002; Nagashima et al., 2010).

Piemontite occurring in the layered manganese deposit of the Tone mine, Nishisonogi Peninsula, Nagasaki, southwest Japan, contains significant amounts of Sr (Fukushima et al., 2003), as well as Sr-bearing piemontites from the various localities referred to above. However, the details of occurrence, chemical composition and structural properties of the Sr-bearing piemontite from the Tone ore deposit have not been studied systematically. In the present study, chemical compositions and crystal structure of the Tone Sr-bearing piemontite were studied by means of electron microprobe analysis (EMPA) and single crystal X-ray structural refinement to deter-

mine the distributions of Sr and Ca in the *A2* and *A1* sites and of transition metal ions in the octahedral sites. Since the occupancies of Fe and Mn in the octahedral sites are not determined using the single crystal X-ray diffraction method, they were complementary determined for the powder sample using the time-of-flight (TOF) neutron Rietveld analyses, where Al occupancy in the octahedral sites determined using X-ray Rietveld analysis was taken into the refinement. The oxidation state and coordination site of Fe cations were determined by the Mössbauer spectroscopic analysis. Based on the results, we examine the relationship between the Sr content in the *A* site and  $M^{3+}$ -cation distribution in the octahedral sites and clarify the effect of Sr and  $M^{3+}$  cation distributions in the *A* and octahedral sites on the  $A\text{-O}_i$  bond lengths and the mean  $M^{3+}\text{-O}$  bond lengths. Finally, the effect of the  $\text{Sr} \leftrightarrow \text{Ca}$  substitution on overall structure of piemontite, which is characteristically represented by the change of the unit-cell parameters and  $\text{Si1-O9-Si2}$  angle, are discussed.

## GEOLOGICAL OUTLINE OF THE TONE ORE DEPOSIT

In Nishisonogi Peninsula, Nagasaki, southwest Japan, Nagasaki metamorphic complex consisting of schists subjected to epidote-glaucophane to epidote-amphibolite facies metamorphism is distributed (Nishiyama, 1990). In this district, some layered manganese ore deposits are intercalated in the Nagasaki metamorphic complex. The ore deposits were mined at the Tone, Muramatsu and Sakiyama mines (Yoshimura, 1952). Braunite and pyrolusite ores are considered to have been mined as manganese resource (Yoshimura, 1952), but the details are not known. Strontioepimontite, hennomartinite and strontiomelane have been also reported from the ores (Fukushima et al., 2003).

## EXPERIMENTAL METHODS

### Piemontite sample preparation

The manganese ores were collected from dump of the Tone mine. The ores have layered structures. The layers showing reddish purple in color contain piemontite as one of major minerals. In this study, piemontite crystals were separated from the ore bearing piemontite as the most dominant phase. Selected piemontite crystals attain up to about 3 mm long and contain hematite inclusions or coexist with hematite. To analyze the chemical composition of piemontite, a thin section of the layer, from which piemontite crystals were separated, was prepared. For the single crystal X-ray diffraction analysis, a piemontite

crystal with  $0.115 \times 0.085 \times 0.04$  mm in dimension was picked up. The piemontite crystals used for the Mössbauer spectral analysis and powder X-ray and TOF neutron diffraction analyses were separated and ground under alcohol in an agate mortar and pestle to obtain a powder sample with fine grains less than 10  $\mu\text{m}$  in size.

#### Electron microprobe analysis of minerals

The chemical compositions of minerals were determined using a JEOL JXA-8230 electron microprobe analyzer at Yamaguchi University, Japan. Operating conditions were as follows: accelerating voltage of 15 kV, a beam current of 20 nA and a beam diameter of 1–10  $\mu\text{m}$ . Wave length-dispersive type X-ray detectors with LiF, PET, and TAP monochromator crystals were used for measurement of the X-ray spectra and X-ray intensities of Si, Ti, Al, Cr, V, Fe, Mn, Mg, Ca, Sr, Ba, Na, K, F, and Cl. The ZAF method was used for data correction. Elements below the detection limit are not shown in Table 1.

#### Single crystal X-ray diffraction analysis

The X-ray diffraction data of the piemontite single crystal were collected at room temperature with graphite-monochromated  $\text{MoK}\alpha$  X-radiation ( $\lambda = 0.71073$  Å) using a Bruker SMART APEX II CCD diffractometer installed at Shimane University, Japan. Preliminary unit-cell parameters and an orientation matrix were obtained from three sets of frames and refined during the integration process of the intensity data. Diffraction data were collected with  $\omega$  scans with different  $\varphi$  settings ( $\varphi$ - $\omega$  scan) (Bruker, 1999). Data were processed using SAINT program (Bruker, 1999). An empirical absorption correction using SADABS program (Sheldrick, 1996) was applied. The systematic absences were consistent with space groups  $P2_1$  and  $P2_1/m$ , and reflection statistics indicated that the observed structure is centrosymmetric. Thus, structural refinement was performed in the space group  $P2_1/m$ , using SHELXL-97 program (Sheldrick, 2015). Scattering factors for neutral atoms were employed. Since the preliminary refinement resulted in the full occupancy of Ca at the  $A1$  site, Al at the  $M2$  site, and Si at the Si1, Si2, and Si3 sites, the site occupancies were fixed to 1.0Ca for the  $A1$  site, 1.0Al for the  $M2$  site and 1.0Si for the Si1, Si2, and Si3 sites. The site occupancies at the  $A2$ ,  $M1$ , and  $M3$  sites were refined with Ca and Sr, Al and Mn, and Mn and Al, respectively. Position of the hydrogen atom was derived from difference-Fourier syntheses and was refined assuming full or half occupancy with fixed  $U_{\text{iso}} = 0.05$  Å<sup>2</sup>. In addition, a bond-distance constraint of O–H = 0.98(2) Å after Franks (1973) was applied.

**Table 1.** Chemical composition of piemontite from the Tone mine\*

	Average	$\sigma$	Maximum
	$n = 23$		Sr content
SiO <sub>2</sub>	36.07	0.69	35.94
TiO <sub>2</sub>	0.02	0.02	0.00
Al <sub>2</sub> O <sub>3</sub>	20.30	1.19	20.77
Cr <sub>2</sub> O <sub>3</sub>	0.01	0.02	0.00
V <sub>2</sub> O <sub>3</sub>	0.01	0.01	0.02
Fe <sub>2</sub> O <sub>3</sub>	5.90	1.24	3.86
Mn <sub>2</sub> O <sub>3</sub>	10.70	1.14	12.19
MgO	0.08	0.03	0.04
CaO	19.49	2.01	16.90
SrO	4.63	2.66	8.48
BaO	0.04	0.05	0.00
Na <sub>2</sub> O	0.01	0.01	0.01
K <sub>2</sub> O	0.01	0.01	0.00
Total	97.28		98.21
Cations per O <sub>12</sub> (OH)			
Si	2.99	0.01	3.00
Ti	0.00	0.00	0.00
Al	1.99	0.09	2.04
Cr	0.00	0.00	0.00
V	0.00	0.00	0.00
Fe <sup>3+</sup>	0.37	0.08	0.24
Mn <sup>3+</sup>	0.68	0.08	0.77
Mg	0.01	0.00	0.01
Ca	1.73	0.15	1.51
Sr	0.22	0.13	0.41
Ba	0.00	0.00	0.00
Na	0.00	0.00	0.00
K	0.00	0.00	0.00
Total	7.99		7.98

\*Cr, Cr<sub>2</sub>O<sub>3</sub>; V, V<sub>2</sub>O<sub>3</sub>; Fe, Fe<sub>2</sub>O<sub>3</sub>; Mn, Mn<sub>2</sub>O<sub>3</sub>.

#### Collection of powder X-ray diffraction data and X-ray Rietveld analysis

The powdered piemontite sample was mounted in a sample holder made of glass, with a cavity measuring  $20 \times 15 \times 0.2$  mm. Following the method of Raudsepp et al. (1990), a straight edge was used to level the sample surface to that of the holder. The surface was then finely serrated several times with a razor blade to randomize the orientation of anisotropic crystals that are aligned during filling. The powder X-ray diffraction data were collected using Rigaku SmartLab X-ray powder diffractometer using  $\text{CuK}\alpha$  radiation ( $\lambda = 1.5418$  Å) and Dtex/Ultra detector with Bragg-Brentano geometry. The X-ray diffraction data was taken between 5.00 and 150.00°  $2\theta$  with a step interval of 0.01°  $2\theta$ . X-ray generator was operated at 40

kV and 200 mA. The crystal structures of the piemontite were refined using the RIETAN-FP program of Izumi and Momma (2007). The atomic coordinates and isotropic displacement parameters of a Sr-bearing piemontite analyzed by Dollase (1969) were used for the initial input. The isotropic displacement parameters for all atoms were fixed during the refinement. The unit-cell parameters determined using a Rigaku PDXL software were used as initial values of the Rietveld analysis. Peaks were defined using Modified split pseudo-Voigt function for relaxed reflections (Izumi and Ikeda, 2000) in RIETAN-FP. Non-linear least-squares calculation using the Marquardt method was followed by the conjugate direction method to check convergence at local minima (Izumi, 1993). The March-Dollase function (Dollase, 1986) was applied to the correction of preferred orientation. Based on the result of the chemical analysis, the occupancies of Ca at the *A1* site and Si at Si1, Si2, and Si3 sites were fixed at unity. The site occupancy at the *A2* site was refined using the following constraint:  $^{42}\text{Sr} = 1.0 - ^{42}\text{Ca}$ . The occupancies of Al and Mn at the octahedral sites were refined using the following constraints:  $^{M1}\text{Mn} = 1.0 - ^{M1}\text{Al}$  and  $^{M3}\text{Al} = 1.0 - ^{M3}\text{Mn}$ , where 'Mn' implies 'Mn + Fe'. At the *M2* site, Al was fixed at unity, because the preliminary refinement indicated that the *M2* site is filled with Al.

### Collection of the TOF neutron data and Rietveld analysis

TOF neutron powder-diffraction data of the piemontite powder sample was measured at room temperature using TOF neutron powder diffractometer at the BL11 beamline in MLF of Japan Proton Accelerator Research Complex (J-PARC) facility (Hattori et al., 2015). The sample of 0.04 g was mounted in a vanadium tube (OD 3mm and ID 2.8mm). Diffraction was detected by a pair of  $^3\text{He}$  PSD detector bank that covers  $2\theta$  of  $90 \pm 11.3^\circ$ , through the radial collimators with a gauge length of 3 mm. Data was collected for 8 h and 45 min on accelerator power of approximately 500 kW. Intensity was corrected using the data of vanadium rod, empty vanadium holder and instrumental background which were measured separately. The Rietveld analysis of the neutron-diffraction data was performed using the Z-Rietveld software (ver. 1.0.2, Oishi et al., 2009; Oishi-Tomiyasu et al., 2012). Peaks were defined using a profile function 0 in Z-Rietveld. Based on the EMPA data and the results of the X-ray Rietveld refinement, Ca at the *A1* site and Si at the Si1, Si2, and Si3 sites were fixed at unity. Site occupancies of Sr and Ca in the *A2* site were refined using the following constraint:  $^{42}\text{Sr} = 1.0 - ^{42}\text{Ca}$ . As mentioned by Ferraris et al. (1989), to obtain the occupancies of Al, Mn, and Fe at the *M1*

and *M3* sites, Al content has to be fixed to the value given by the X-ray structural refinement. Thus, in the preliminary neutron Rietveld refinement, the occupancies of Al at the *M1* and *M3* sites were fixed to those determined by the X-ray Rietveld analysis, and the occupancies of Mn and Fe at these sites were refined. As a result of the refinement, it was found that the *M1* site has Mn but no Fe, and that both Mn and Fe are present in the *M3* site. Therefore, in the final refinement, the site occupancy at the *M1* site was refined with Al and Mn; and that at the *M3* site was refined with Mn and Fe using the fixed Al occupancy by the X-ray data. At the *M2* site, Al was fixed at unity based on the result by the X-ray Rietveld analysis.

### $^{57}\text{Fe}$ Mössbauer spectroscopic analysis

The  $^{57}\text{Fe}$  Mössbauer spectrum of the powder sample of piemontite, with ~ 20 mg in weight, was measured at room temperature, using 370 MBq  $^{57}\text{Co}$  in Pd as a source. Mössbauer data were obtained using a constant acceleration spectrometer fitted with a 1024 channel analyzer. The isomer shift was referred to a standard metallic iron foil, which was also used to calibrate the Doppler velocity. The spectrum was fitted to Lorentzians using the least squares method with line widths and intensities constrained to be equal for each doublet. The QBMOSS program written by Akasaka and Shinno (1992) was used for computer analysis. The quality of the fit was judged using the  $\chi^2$  value and standard deviations of Mössbauer parameters.

## RESULTS

### Chemical composition of the Tone piemontite

Chemical composition of the Tone piemontite is shown in Table 1, where total Fe and Mn are shown as  $\text{Fe}_2\text{O}_3$  and  $\text{Mn}_2\text{O}_3$ . The trivalent oxidation state of Fe was proved by the Mössbauer spectroscopic analysis, as shown later, and that of Mn ions was evaluated from stoichiometry of the chemical composition. The SrO content is  $4.63 \pm 2.66$  wt% on average, but attains 8.48 wt% at maximum, corresponding to 0.41 apfu  $[\text{O}_{12}(\text{OH})]$ . Rather large standard deviation of the average SrO content is due to the zonal structure with Sr-poorer core and Sr-rich overgrowths (Fig. 1). The chemical formula derived from the average composition by 23 point analytical data is  $[\text{Ca}_{1.73(15)}\text{Sr}_{0.22(13)}]_{\Sigma 1.95}[\text{Al}_{1.99(9)}\text{Mn}_{0.68(8)}\text{Fe}_{0.37(8)}\text{Mg}_{0.01(0)}]_{\Sigma 3.05}\text{Si}_{2.99(1)}\text{O}_{12}(\text{OH})$  ( $Z = 2$ ), which was applied to the powder piemontite sample used for the Mössbauer spectroscopic and the X-ray and neutron Rietveld analyses in this study.

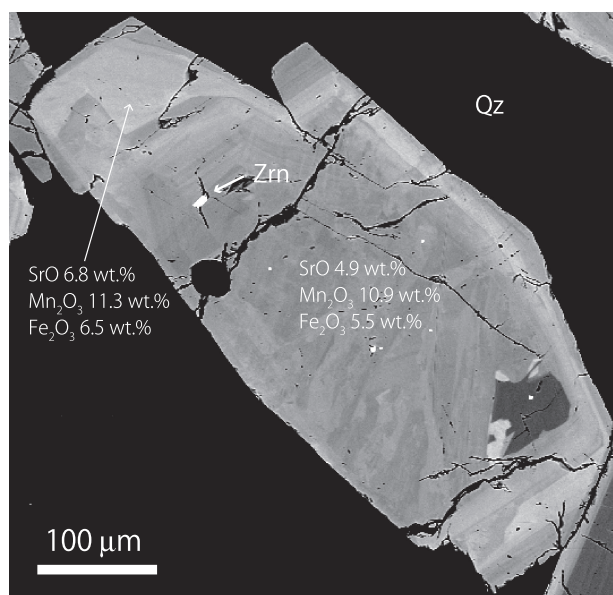


**Figure 1.** Backscattered electron (BSE) image of piemontite with zircon (Zrn) and quartz (Qz). The abbreviations of mineral are used after Whitney and Evans (2010).

### Single crystal X-ray structural refinement

Crystallographic data and refined parameters in the single crystal X-ray structural refinement of the piemontite single crystal are summarized in Table 2. The refined site occupancies, atomic positions and anisotropic atomic displacement parameters are listed in Table 3. The interatomic distances, selected angles, volumes of the coordination polyhedra and site distortion parameters are listed in Table 4. The respective errors in all tables are shown by the standard deviation of  $1\sigma$ .

The refinement was converged to  $R_1 = 2.51\%$ . The determined unit cell parameters are  $a = 8.8942(1)$ ,  $b = 5.6540(1)$ ,  $c = 10.1928(2)$  Å, and  $\beta = 115.100(1)^\circ$ . The site occupancies are  $\text{Ca}_{0.711(3)}\text{Sr}_{0.289}$  at the  $A2$  site,  $\text{Al}_{0.898(4)}\text{Mn}_{0.102}$  at the  $M1$  site, and  $\text{Mn}_{0.949(4)}\text{Al}_{0.051}$  at the  $M3$  site, where the occupancy of Mn includes that of Fe. The  $A1$  site is only occupied by Ca and the smallest octahedral  $M2$  site is fulfilled with aluminum. The Sr population in the  $A2$  site, 0.289 apfu, is more than the average composition, 0.23 apfu, by EMPA, whereas the (Mn + Fe) content, 1.051 apfu, agrees with the EMPA data, 1.05 apfu.

### X-ray and TOF neutron Rietveld analyses

Details of data collection for the X-ray and TOF neutron Rietveld analyses, the refined unit cell parameters,  $R$ -factors, goodness-of-fit ( $S = R_{\text{wp}}/R_e$ ) and the Durbin-Watson  $d$  statistic are listed in Table 5. The refined powder patterns by the X-ray and TOF neutron diffractions are given

**Table 2.** Details of single-crystal X-ray diffraction data collection and refined results of piemontite crystal

Crystal size (mm)	0.115 × 0.085 × 0.040	
Space group	$P2_1/m$	
Cell parameters	$a$ (Å)	8.8942(1)
	$b$ (Å)	5.6540(1)
	$c$ (Å)	10.1928(2)
	$\beta$ (°)	115.100(1)
	$V$ (Å <sup>3</sup> )	464.17(2)
$Z$	2	
$D_{\text{calc}}$ (g/cm <sup>3</sup> )	3.62	
$\mu$ (mm <sup>-1</sup> )	5.76	
Collected reflections	8659	
Unique reflections	2417	
$R_{\text{int}}$	0.0316	
$R\sigma$	0.0303	
$\theta_{\text{min}}-\theta_{\text{max}}$ (°)	2.6-36.3	
Miller index limit	-14 ≤ $h$ ≤ 14, -9 ≤ $k$ ≤ 9, -15 ≤ $l$ ≤ 16	
$R_1$	0.0251	
$wR2$	0.0632	
No. of parameters	123	
Weighting scheme*	$w = 1/[\sigma^2(F_o^2) + (0.0311P)^2 + 0.09P]$	
$\Delta\rho_{\text{max}}$ (e Å <sup>-3</sup> )	0.63 (0.73 Å from O2)	
$\Delta\rho_{\text{min}}$ (e Å <sup>-3</sup> )	-0.57 (0.50 Å from A2)	

\* The function of the weighting scheme is  $w = 1/[\sigma^2(F_o^2) + (a \cdot P)^2 + b \cdot P]$ , where  $P = [\text{Max}(F_o^2) + 2F_c^2]/3$ , and the parameters  $a$  and  $b$  are chosen to minimize the differences in the variances for reflections in different ranges of intensity and diffraction angle.

in Figure 2a and b, respectively. The site occupancies and atomic positions are listed in Table 6. Figure 3 shows the crystal structure of the Tone piemontite.

The refinement of the powder X-ray diffraction data was reduced to  $R_{\text{wp}} = 2.95$ ,  $R_e = 2.13$  and  $S = 1.38$ . The refined unit cell parameters are  $a = 8.8769(3)$ ,  $b = 5.66844(7)$ ,  $c = 10.1881(4)$  Å, and  $\beta = 115.199(3)^\circ$ . The determined site occupancies at the  $A2$ ,  $M1$ , and  $M3$  sites are  $\text{Ca}_{0.795(6)}\text{Sr}_{0.205}$ ,  $\text{Al}_{0.909(7)}\text{Mn}_{0.091}$ , and  $\text{Mn}_{0.80(1)}\text{Al}_{0.20}$ , respectively, where the occupancy of Mn includes that of Fe.

The refinement of the TOF neutron data was reduced to  $R_{\text{wp}} = 2.11$ ,  $R_e = 0.88$  and  $S = 2.39$  and resulted in the unit cell parameters of  $a = 8.8817(2)$ ,  $b = 5.6744(2)$ ,  $c = 10.1885(3)$  Å, and  $\beta = 115.244(4)^\circ$ ; the site occupancies of  $\text{Ca}_{0.791(5)}\text{Sr}_{0.209}$ ,  $\text{Al}_{0.902(5)}\text{Mn}_{0.098}$ , and  $\text{Mn}_{0.534(5)}\text{Fe}_{0.267}\text{Al}_{0.20}$  at the  $A2$ ,  $M1$  and  $M3$  sites, respectively.

**Table 3.** Site occupancies, atomic positions and equivalent displacement parameters ( $\text{\AA}^2$ ) determined by the single crystal X-ray diffraction analysis

Site	$W^*$	Occupancy	$x$	$y$		$U_{\text{eq}}$	$U_{11}$	$U_{22}$	$U_{33}$
A1	2e	Ca <sub>1.0</sub>	0.75991(5)	3/4	0.15427(4)	0.01048(9)	0.01389(18)	0.0103(2)	0.01028(16)
A2	2e	Ca <sub>0.711(3)</sub> Sr <sub>0.289</sub>	0.59902(4)	3/4	0.42349(3)	0.01163(10)	0.01193(15)	0.01472(18)	0.00757(13)
M1	2a	Al <sub>0.898(4)</sub> Mn <sup>**</sup> <sub>0.102</sub>	0	0	0	0.00530(16)	0.0057(2)	0.0041(3)	0.0060(2)
M2	2c	Al <sub>1.0</sub>	0	0	1/2	0.00644(12)	0.0063(2)	0.0052(3)	0.0077(2)
M3	2e	Mn <sup>**</sup> <sub>0.949(4)</sub> Al <sub>0.051</sub>	0.29338(4)	1/4	0.22173(3)	0.00637(9)	0.00535(13)	0.00667(16)	0.00691(13)
Si1	2e		0.33947(7)	3/4	0.04481(6)	0.00634(11)	0.0068(2)	0.0061(3)	0.0065(2)
Si2	2e		0.68522(7)	1/4	0.27649(6)	0.00631(11)	0.0064(2)	0.0061(3)	0.0067(2)
Si3	2e		0.18245(7)	3/4	0.31719(6)	0.00619(10)	0.0065(2)	0.0061(3)	0.0067(2)
O1	4f		0.23393(13)	0.9932(2)	0.03900(11)	0.00954(19)	0.0095(4)	0.0070(5)	0.0135(4)
O2	4f		0.30224(13)	0.9806(2)	0.35353(11)	0.00953(19)	0.0097(4)	0.0086(5)	0.0102(4)
O3	4f		0.79485(13)	0.0146(2)	0.34131(11)	0.00959(19)	0.0085(4)	0.0061(5)	0.0113(4)
O4	2e		0.05408(18)	1/4	0.12974(15)	0.0074(3)	0.0083(6)	0.0069(7)	0.0074(5)
O5	2e		0.04080(18)	3/4	0.14551(15)	0.0083(3)	0.0077(6)	0.0094(7)	0.0073(5)
O6	2e		0.06516(18)	3/4	0.40564(16)	0.0079(3)	0.0106(6)	0.0057(7)	0.0105(6)
O7	2e		0.51485(18)	3/4	0.17643(16)	0.0119(3)	0.0086(6)	0.0137(8)	0.0109(6)
O8	2e		0.52543(19)	1/4	0.31044(17)	0.0124(3)	0.0094(6)	0.0161(8)	0.0134(6)
O9	2e		0.6296(2)	1/4	0.10236(17)	0.0171(3)	0.0221(8)	0.0228(10)	0.0107(6)
O10	2e		0.08134(18)	1/4	0.42865(15)	0.0076(3)	0.0093(6)	0.0070(7)	0.0083(6)
H10	2e		0.043(5)	1/4	0.3233(6)	0.05 ( $U_{\text{iso}}$ )			

**Table 3.** (Continued)

Site	$U_{23}$	$U_{13}$	$U_{12}$
A1	0	0.00803(14)	0
A2	0	0.00348(10)	0
M1	-0.00050(18)	0.00238(18)	-0.00054(18)
M2	0.0000(2)	0.00285(19)	0.0000(2)
M3	0	0.00244(10)	0
Si1	0	0.00310(17)	0
Si2	0	0.00298(17)	0
Si3	0	0.00354(17)	0
O1	0.0010(4)	0.0062(4)	0.0015(4)
O2	-0.0005(4)	0.0042(3)	-0.0021(4)
O3	-0.0011(4)	0.0014(3)	0.0009(4)
O4	0	0.0036(5)	0
O5	0	0.0026(5)	0
O6	0	0.0074(5)	0
O7	0	0.0018(5)	0
O8	0	0.0067(5)	0
O9	0	0.0111(6)	0
O10	0	0.0053(5)	0
H10			

\* Multiplicity and Wyckoff letter.

\*\* Mn + Fe.

The refined Sr occupancies using the powder X-ray and TOF neutron diffraction data are consistent with each other, and the Sr population in the A2 site given from the refined Sr occupancy, 0.21 apfu, is close to that of the

average composition by EMPA, 0.23 apfu. The sum of Mn and Fe populations derived from the X-ray diffraction data, 0.891 apfu [= 0.091(M1) + 0.80(M3)], is also close to that from the neutron diffraction data, 0.899 apfu [= 0.098Mn(M1) + 0.534Mn(M3) + 0.267Fe(M3)], whereas they are somewhat less than that of EMPA data, Mn<sup>3+</sup> + Fe<sup>3+</sup> = 1.05 apfu. A possible reason may be attributed to the limited number of the EMPA analysis data. The neutron Rietveld analysis results in Mn population of 0.632 apfu [= 0.098Mn(M1) + 0.534Mn(M3)] and Fe population of 0.267 apfu [= Fe(M3)], which is fairly consistent with the Mn<sup>3+</sup> and Fe<sup>3+</sup> contents (Mn<sup>3+</sup> = 0.68 apfu and Fe<sup>3+</sup> = 0.37 apfu) of the average chemical composition by EMPA (Table 1).

### <sup>57</sup>Fe Mössbauer spectroscopy

<sup>57</sup>Fe Mössbauer spectra and hyperfine parameters are shown in Figure 4 and Table 7, respectively. The spectrum consists of three doublets: the doublet AA' with isomer shift ( $IS$ ) = 0.35 and quadrupole splitting ( $QS$ ) = 2.19 mm/s; the doublet BB' with  $IS$  = 0.37 and  $QS$  = 1.93 mm/s; and the doublet CC' with  $IS$  = 0.18 and  $QS$  = 1.08 mm/s. According to the published Mössbauer studies on the epidote minerals (e.g., Liebscher, 2004; Nagashima and Akasaka, 2010), doublets with  $IS$  = 0.24–0.44 and  $QS$  = 1.89–2.32 mm/s and with  $IS$  = 0.22–0.36 and  $QS$  = 1.46–1.67 mm/s are assigned to Fe<sup>3+</sup> at the M3 and M1 sites,

**Table 4.** Selected interatomic distances (Å), bond angles (°), volume of coordination polyhedra (Å<sup>3</sup>) and distortion parameters for the octahedral sites\*

A1-	O1	×2	2.467(1)	M1-	O1	×2	1.946(1)	M3-	O1	×2	2.241(1)
	O3	×2	2.338(1)		O4	×2	1.8543(9)		O2	×2	2.010(1)
	O5		2.538(2)		O5	×2	1.968(1)		O4		1.928(2)
	O7		2.285(2)				Ave. 1.923		O8		1.869(2)
	O6		2.834(2)	O1-M1-O4			86.44(5)				Ave. 2.050
	O9	×2	3.0157(6)	O1-M1-O5			90.43(5)	O1-M3-O1'			80.78(6)
			Ave. 2.589	O4-M1-O5			95.79(4)	O1-M3-O2			89.60(4)
								O1-M3-O4			76.89(4)
A2-	O2	×2	2.753(1)	M2-	O3	×2	1.857(1)	O1-M3-O8			102.99(5)
	O2'	×2	2.562(1)		O6	×2	1.9318(9)	O2-M3-O2'			98.53(6)
	O3	×2	2.686(1)		O10	×2	1.8699(9)	O2-M3-O4			92.71(4)
	O7		2.303(2)				Ave. 1.886	O2-M3-O8			87.39(4)
	O10		2.592(2)	O3-M2-O6			89.45(6)				
	O8	×2	3.0180(6)	O3-M2-O10			91.54(6)	O10...O4			2.952(2)
			Ave. 2.693	O6-M2-O10			96.44(4)	Si1-O9-Si2			155.3(1)
Si1-	O1	×2	1.652(1)	Si2-	O3	×2	1.616(1)	Si3-	O2	×2	1.624(1)
	O7		1.568(2)		O8		1.599(2)		O5		1.667(2)
	O9		1.636(2)		O9		1.628(2)		O6		1.643(2)
			Ave. 1.627				Ave. 1.615				Ave. 1.640
O1-Si1-O1'			112.71(8)	O3-Si2-O3'			110.86(8)	O2-Si3-O2'			106.79(8)
O1-Si1-O7			112.01(5)	O3-Si2-O8			110.43(5)	O2-Si3-O5			111.72(5)
O1-Si1-O9			106.33(5)	O3-Si2-O9			107.30(5)	O2-Si3-O6			112.50(5)
O7-Si1-O9			106.95(9)	O8-Si2-O9			110.43(9)	O5-Si3-O6			101.71(8)

\* $DI(\text{oct}) = 1/6 \sum |R_i - R_{\text{av.}}|/R_{\text{av.}}$  ( $R_i$ , each bond length;  $R_{\text{av.}}$ , average distance for an octahedron) (Baur, 1974).

$\langle \lambda_{\text{oct}} \rangle = \sum_{i=1}^6 (l_i - l_0)^2 / 6$  ( $l_i$ , each bond length;  $l_0$ , center-to-vertex distance for an octahedron with  $O_h$  symmetry, whose volume is equal to that of a distorted octahedron with bond lengths  $l_i$ ) (Robinson et al., 1971).

$\sigma_{\theta}(\text{oct})^2 = \sum_{i=1}^{12} (\theta_i - 90^\circ)^2 / 11$  ( $\theta_i$ , O-M-O angle) (Robinson et al., 1971).

respectively. Therefore, the doublets AA' and BB' are assigned to Fe<sup>3+</sup> at the M3 site. In contrast, the doublet CC' with  $IS = 0.18$  and  $QS = 1.08$  mm/s and very broad peak width ( $FWHH$ ) of 0.81 mm/s are not assigned to Fe<sup>3+</sup> nor Fe<sup>2+</sup> in epidote minerals. Since the powder X-ray and neutron diffraction analyses indicated that the piemontite powder sample contained a very small amount of quartz as an impurity but no Fe-bearing impurity, an undetectable amount of Fe-rich impurity, such as Fe<sup>3+</sup>-rich hydroxide, might have been contaminated in the powder sample. The result of the Mössbauer spectroscopic analysis that Fe<sup>3+</sup> is distributed only in the M3 site but not the M1 site proves that of the neutron Rietveld analysis.

The presence of two doublets, with  $IS = 0.34$  and  $QS = 2.04$  mm/s and with  $IS = 0.39$  and  $QS = 1.95$  mm/s, assigned to Fe<sup>3+</sup> at the M3 site has been reported for synthetic epidote with  $0.5 \leq \text{Fe} \leq 0.7$  apfu (Fehr and Heuss-Abichler, 1997). Two doublets with  $IS = 0.34$  and  $QS = 2.16$ -2.22 mm/s and with  $IS = 0.36$ -0.37 and  $QS = 1.90$ -

1.97 mm/s due to Fe<sup>3+</sup> at the M3 sites were also found in the synthetic Ca<sub>2</sub>(Al<sub>2.10</sub>-2.15Mn<sub>0.78</sub>-0.73Fe<sub>0.12</sub>)Si<sub>3</sub>O<sub>12</sub>(OH)-piemontite (Nagashima and Akasaka, 2010). Although aforementioned previous studies supposed a miscibility gap at the compositions of their synthetic epidote and piemontite, the two Fe<sup>3+</sup> doublets assigned to the M3 site in the Tone piemontite may be attributed to the chemical heterogeneity of the piemontite crystals separated for the powder sample.

## DISCUSSION

### Site populations of Sr and transition metal ions in the studied Tone piemontite

Based on the site occupancies refined using the single crystal X-ray diffraction data, the structural formula of the Tone piemontite single crystal is derived as <sup>A2</sup>(Ca<sub>0.711(3)</sub>Sr<sub>0.289</sub>)<sup>A1</sup>Ca<sup>M1</sup>(Al<sub>0.898(4)</sub>Mn<sub>0.102</sub>)<sup>M2</sup>Al<sup>M3</sup>(Mn<sub>0.949(4)</sub>Al<sub>0.051</sub>)

**Table 5.** Details of powder X-ray and TOF neutron diffraction data collection and refined results of piemontite

	X-ray	TOF neutron
2 $\theta$ range (°)	5-150	-
$d$ range (Å)	-	0.55-5.28*
Space group	$P2_1/m$	
$a$ (Å)	8.8769(3)	8.8817(2)
$b$ (Å)	5.66844(7)	5.6744(2)
$c$ (Å)	10.1881(4)	10.1885(3)
$\beta$ (°)	115.199(3)	115.244(4)
$V$ (Å <sup>3</sup> )	463.86(3)	464.45(3)
$R_B$ (%)**	2.05	6.63
$R_F$ (%)**	1.16	4.22
$R_p$ (%)**	2.20	1.65
$R_{wp}$ (%)**	2.95	2.11
$R_e$ (%)**	2.13	0.88
$S^{**}$	1.38	2.39
D-W $d^{**}$	0.727	0.568
$r^{**}$	1.037	1.035
Mass fraction		
Piemontite	0.991	0.948
Quartz	0.009	0.052

\* Corresponding to range of TOF data 5200-49998.

\*\*  $R_B$ ,  $R$ -Bragg factor;  $R_F$ ,  $R$ -structure factor;  $R_p$ ,  $R$ -pattern;  $R_{wp}$ ,  $R$ -weighted pattern;  $R_e$ ,  $R$ -expected.

$S$  ( $=R_{wp}/R_e$ ), Goodness of fit (Young, 1993); D-W  $d$ , Durbin-Watson  $d$ -statistic (Hill and Flack, 1987);  $r$ , Preferred-orientation parameter in the March-Dollase function.

$\text{Si}_3\text{O}_{12}(\text{OH})$ , where  $\text{Mn}^*$  implies sum of Mn and Fe. The results of the neutron Rietveld refinement and Mössbauer spectroscopic analysis for the powder sample indicate that the  $M1$  site is occupied by  $\text{Al}^{3+}$  and  $\text{Mn}^{3+}$  but not by  $\text{Fe}^{3+}$ . Therefore,  $\text{Mn}^*$  at the  $M1$  site for the piemontite single crystal is also regarded to be only Mn, and the  $M1$  site population is concluded as  $^{M1}[\text{Al}_{0.898(4)}\text{Mn}_{0.102}^{3+}]$  in apfu, which is in agreement with  $^{M1}[\text{Al}_{0.902(5)}\text{Mn}_{0.098}]$  in apfu of the powder sample. Consequently, the  $M3$  site in the piemontite single crystal is filled with Al, Mn, and Fe, which is in agreement with the analytical result of the powder sample. Applying the Mn:Fe-ratio in the  $M3$  site for the powder piemontite sample,  $\text{Mn}0.534(5):\text{Fe}0.267$  in apfu, to the piemontite single crystal in the present study, the  $M3$  site population of the piemontite single crystal is derived as  $^{M3}[\text{Mn}_{0.633}\text{Fe}_{0.316}\text{Al}_{0.051}]$  in apfu. Since Fe and Mn are trivalent in oxidation state, respectively, the structural formula of the piemontite single crystal is built as  $^{42}[\text{Ca}_{0.711(3)}\text{Sr}_{0.289}]^{41}\text{Ca}^{M1}[\text{Al}_{0.898(4)}\text{Mn}_{0.102}^{3+}]^{M2}\text{Al}^{M3}[\text{Mn}_{0.633}^{3+}\text{Fe}_{0.316}\text{Al}_{0.051}]\text{Si}_3\text{O}_{12}(\text{OH})$ . The obtained total  $\text{Mn}^{3+}$  and  $\text{Fe}^{3+}$ , 0.735 and 0.316 apfu, respectively, are fairly close

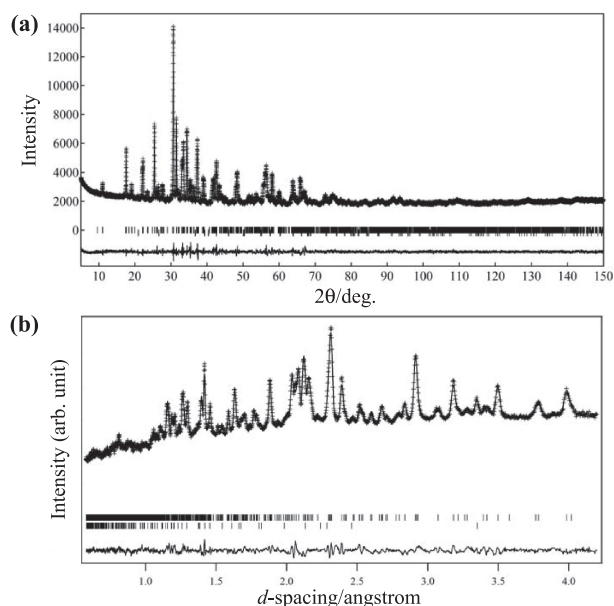


**Figure 2.** Rietveld refinement plots with X-ray ( $\text{CuK}\alpha$ ) (a) and TOF neutron (b) diffraction patterns of piemontite. The sample was refined with piemontite and quartz. The crosses are the observed data, the solid line is the calculated pattern, and the vertical bars mark all possible reflections. Upper and lower bar marks are piemontite and quartz, respectively. The difference between the observed and calculated patterns is shown at the bottom.

to those of the EMPA data, 0.68(8)  $\text{Mn}^{3+}$  and 0.37(8)  $\text{Fe}^{3+}$  apfu (Table 1).

It has been suggested that piemontites rich in Sr and/or Ba tend to be rich in  $\text{Mn}^{3+}$  and  $\text{Fe}^{3+}$ : in piemontite from the Fukuyama manganese iron ore deposit, Tokoro, Hokkaido, Japan,  $\text{Sr}/(\text{Sr} + \text{Ca})$ ,  $\text{Mn}^{3+}/(\text{Al} + \text{Mn}^{3+} + \text{Fe}^{3+})$ , and  $(\text{Mn}^{3+} + \text{Fe}^{3+})/(\text{Al} + \text{Mn}^{3+} + \text{Fe}^{3+})$  ratios attain 0.48, 0.51, and 0.58, respectively, corresponding to 0.96 Sr apfu, 1.53  $\text{Mn}^{3+}$  apfu and, 1.74 ( $\text{Mn}^{3+} + \text{Fe}^{3+}$ ) apfu, respectively (Togari et al., 1988; Akasaka et al., 1988); in the Kalahari manganese field, South Africa, the Sr,  $\text{Mn}^{3+}$ , and  $\text{Fe}^{3+}$  contents in tweddillite with the lowest Al concentration are 0.99, 1.52, and 0.41 apfu, respectively (Armbruster et al., 2002); and from Sambagawa metamorphic rocks, central Shikoku, Japan, piemontite with 0.58 apfu Sr, 1.42 apfu  $\text{Mn}^{3+}$ , and 0.81 apfu  $\text{Fe}^{3+}$  and ( $\text{Mn}^{3+} + \text{Fe}^{3+}$ ) of 2.23 apfu was reported (Enami and Banno, 2001). In fact, Sr-rich zone within the Tone piemontite crystal tends to be richer in Mn and Fe than Sr-poor core and zone, as shown in Figure 1. However, the  $\text{Mn}^{3+}$ , and  $\text{Fe}^{3+}$  and ( $\text{Mn}^{3+} + \text{Fe}^{3+}$ ) contents in the Tone piemontite with Sr = 0.289 apfu are 0.735, and 0.316 and 1.051 apfu, respectively, and less than those of the piemontites with lower Sr contents from St. Marcel, Italy, and from the Kamisugai deposit, central Shikoku, Japan: in the former,  $\text{Mn}^{3+} = 0.78$ , and  $\text{Fe}^{3+} =$

**Table 6.** Refined site occupancies, atomic positions and site occupancies obtained by X-ray and TOF neutron Rietveld analyses\*

Site		Occupancy	<i>x</i>	<i>y</i>	<i>z</i>	<i>B</i> *
A1	X-ray	Ca <sub>1.0</sub>	0.7574(5)	3/4	0.1460(5)	0.77
	TOF	Ca <sub>1.0</sub>	0.76282(10)	3/4	0.1644(11)	
A2	X-ray	Ca <sub>0.795(6)</sub> Sr <sub>0.205</sub>	0.5966(5)	3/4	0.4238(4)	0.81
	TOF	Ca <sub>0.791(5)</sub> Sr <sub>0.209</sub>	0.60099(10)	3/4	0.42289(9)	
M1	X-ray	Al <sub>0.909(7)</sub> Mn <sup>**</sup> <sub>0.091</sub>	0	0	0	0.47
	TOF	Al <sub>0.902(5)</sub> Mn <sub>0.098</sub>	0	0	0	
M2	X-ray	Al <sub>1.0</sub>	0	0	1/2	0.56
	TOF	Al <sub>1.0</sub>	0	0	1/2	
M3	X-ray	Mn <sup>**</sup> <sub>0.80(1)</sub> Al <sub>0.20</sub>	0.2964(5)	1/4	0.2210(4)	0.39
	TOF	Mn <sub>0.534(5)</sub> Fe <sub>0.267</sub> Al <sub>0.20</sub>	0.2935(4)	1/4	0.222(3)	
Si1	X-ray	Si <sub>1.0</sub>	0.3402(7)	3/4	0.0457(6)	0.52
	TOF	Si <sub>1.0</sub>	0.33919(11)	3/4	0.05079(10)	
Si2	X-ray	Si <sub>1.0</sub>	0.6891(8)	1/4	0.2736(7)	0.51
	TOF	Si <sub>1.0</sub>	0.67937(13)	1/4	0.27346(11)	
Si3	X-ray	Si <sub>1.0</sub>	0.1832(7)	3/4	0.3117(7)	0.35
	TOF	Si <sub>1.0</sub>	0.17187(10)	3/4	0.30646(10)	
O1	X-ray		0.2370(10)	0.9898(14)	0.0331(8)	0.81
	TOF		0.23426(6)	0.99386(11)	0.03838(5)	
O2	X-ray		0.3006(10)	0.9855(12)	0.3478(9)	0.80
	TOF		0.30371(6)	0.98643(8)	0.35076(6)	
O3	X-ray		0.7859(11)	0.0083(13)	0.3419(8)	0.81
	TOF		0.79504(6)	0.01826(8)	0.342(4)	
O4	X-ray		0.0563(13)	1/4	0.1440(12)	0.59
	TOF		0.05493(7)	1/4	0.13684(8)	
O5	X-ray		0.0440(11)	3/4	0.1489(13)	0.70
	TOF		0.04266(7)	3/4	0.1427(10)	
O6	X-ray		0.0712(13)	3/4	0.4117(14)	0.62
	TOF		0.06056(9)	3/4	0.39544(9)	
O7	X-ray		0.5214(13)	3/4	0.1724(10)	0.80
	TOF		0.5201(8)	3/4	0.17851(8)	
O8	X-ray		0.5221(13)	1/4	0.3188(12)	0.92
	TOF		0.51521(9)	1/4	0.31032(9)	
O9	X-ray		0.6132(14)	1/4	0.0987(13)	0.99
	TOF		0.62041(8)	1/4	0.09637(8)	
O10	X-ray		0.0870(13)	1/4	0.4308(12)	0.60
	TOF		0.08552(8)	1/4	0.44344(8)	
H10	TOF		0.04978(18)	1/4	0.31779(17)	3.95

\* Isotropic thermal parameters, *B*, were fixed at the values obtained by Dollase (1969).

\*\* Mn + Fe.

0.35 and (Mn<sup>3+</sup> + Fe<sup>3+</sup>) = 1.13 apfu against Sr = 0.16 apfu (Ferraris et al., 1989); in the latter (Mn<sup>3+</sup> + Fe<sup>3+</sup>) = 1.17 apfu against Sr = 0.19 apfu (Nagashima et al., 2010). Therefore, piemontite with high Sr content is not necessarily richer in (Mn<sup>3+</sup> + Fe<sup>3+</sup>) content than Sr-poor piemontite. The presence of niigataite, Sr-analogue of clinzoisite (Miyajima et al. 2003), also supports this consideration. Above result is understandable by the proposed factors controlling Sr, REE and transition element contents in pie-

montite and epidote, that is (1) the chemical composition of the host rocks, (2) the local availability of these elements, and (3) hydrothermal and/or metamorphic fluids supplying these elements, as discussed by e.g., Togari et al. (1988) and Akasaka et al. (1988) for Mn<sup>3+</sup>, Fe<sup>3+</sup>, and Sr; Nagashima et al. (2010) for Mn, Fe, Sr, and REE; Nagashima et al. (2006) for Cr, Sr, and REE; and Treloar (1987) and Torres-Ruiz et al. (2003) for Cr. In the experimental studies on piemontite in the join Ca<sub>2</sub>Al<sub>3</sub>Si<sub>3</sub>O<sub>12</sub>

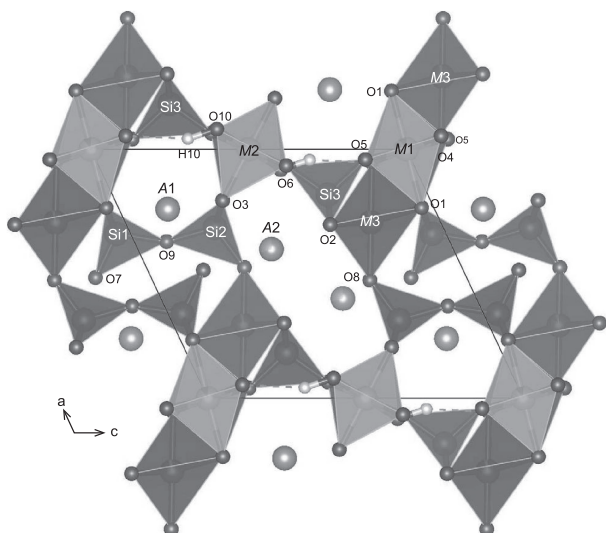


**Figure 3.** Crystal structure of Sr-rich piemontite projected down [010] using the program VESTA3 (Momma and Izumi, 2011).

(OH)-Ca<sub>2</sub>Mn<sup>3+</sup>Si<sub>3</sub>O<sub>12</sub>(OH) by Langer et al. (2002) and Nagashima and Akasaka (2004), piemontites containing as much as 1.48 and 1.26 Mn<sup>3+</sup> apfu, respectively, were synthesized from the starting materials of Ca<sub>2</sub>Al<sub>1.2</sub>Mn<sub>1.8</sub>Si<sub>3</sub>O<sub>12</sub>(OH) and Ca<sub>2</sub>Al<sub>1.5</sub>Mn<sub>1.5</sub>Si<sub>3</sub>O<sub>12</sub>(OH) in composition, respectively, indicating that the Mn<sup>3+</sup>-rich piemontite is formed from the starting material with high Mn<sup>3+</sup> content irrespective of whether Sr is present or absent. The Mn<sup>3+</sup> content in the host material, thus, is the most important factor for the formation of Mn<sup>3+</sup>-rich piemontite. Therefore, Sr, REE and transition element contents in piemontite and epidote depend on their activity in the wall rocks and metamorphic or hydrothermal fluids, but Sr content in piemontite and epidote is not an essential factor for the transition element contents.

On the other hand, at first glance, the Sr content appears to affect the (Mn + Fe) content in the M1 and M3 sites. The intracrystalline partitioning coefficient for (Mn<sup>3+</sup> + Fe<sup>3+</sup>)-Al partitioning, defined as  $K_D = [(Fe^{3+} + Mn^{3+})/Al]^{M1}/[(Fe^{3+} + Mn^{3+})/Al]^{M3}$ , in the Tone piemontite is calculated as 0.006 (Fig. 5). Since the  $K_D$  values for

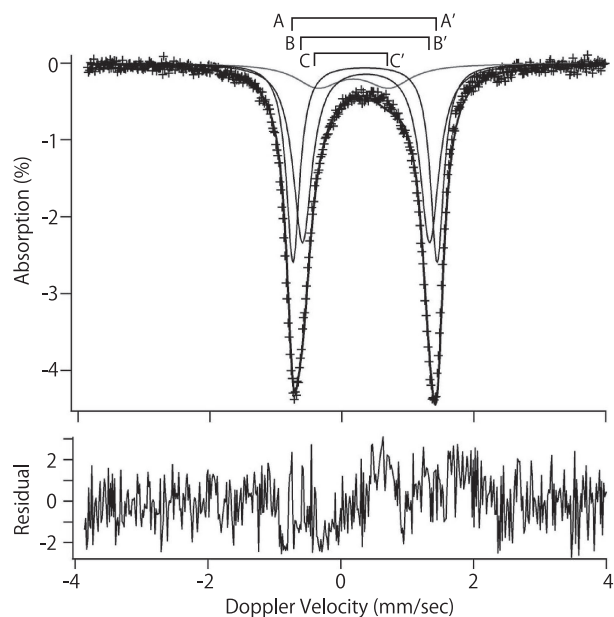


**Figure 4.** <sup>57</sup>Fe Mössbauer spectrum of piemontite at 293K. The refined Mössbauer hyperfine parameters are listed in Table 7.

(Mn<sup>3+</sup> + Fe<sup>3+</sup>)-Al partitioning in the synthetic Ca<sub>2</sub>Al<sub>2</sub>(Fe<sup>3+</sup>, Mn<sup>3+</sup>)Si<sub>3</sub>O<sub>12</sub>(OH)-epidote and piemontite are 0.05–0.13 (Nagashima and Akasaka, 2010), the  $K_D$  value of the Tone piemontite is significantly lower than those of Sr-free Ca-epidote and Ca-piemontite (Fig. 5), indicating that the M3 site preference of (Mn<sup>3+</sup> + Fe<sup>3+</sup>) in the Tone piemontite is stronger than that in the Sr-free Ca-epidote-piemontite series. However, the  $K_D$  value for Mn<sup>3+</sup>-Al partitioning [ $K_D = (Mn^{3+}/Al)^{M1}/(Mn^{3+}/Al)^{M3}$ ] in the Tone piemontite is 0.066, which is in a range of the values for the synthetic Ca-piemontites, that is  $K_D = 0.063$ –0.080 after Langer et al. (2002) and  $K_D = 0.038$ –0.063 after Nagashima and Akasaka (2004). Moreover, the Mn<sup>3+</sup> occupancies at M3 and M1 sites in the Tone piemontite, 0.633 and 0.102, respectively, agree to the calculated values, 0.63 for the M3 site and 0.08 for the M1 site using the regression equations on the Mn<sup>3+</sup> occupancy at the M3 and M1 sites against total Mn<sup>3+</sup> apfu in the synthetic Ca<sub>2</sub>(Al, Mn<sup>3+</sup>)<sub>3</sub>Si<sub>3</sub>O<sub>12</sub>(OH)-piemontites formulated by Nagashima and

**Table 7.** Mössbauer hyperfine parameters of Tone piemontite\*

	<i>IS</i> (mm/s)	<i>QS</i> (mm/s)	<i>FWHH</i> (mm/s)	Area Ratio (%)	Assignment
AA'	0.351(2)	2.185(5)	0.244(9)	38(3)	Fe <sup>3+</sup> (M3) in piemontite
BB'	0.367(6)	1.93(1)	0.35(1)	48(2)	Fe <sup>3+</sup> (M3) in piemontite
CC'	0.18(2)	1.08(4)	0.81(6)	14(1)	Unassignable
$\chi^2$ /Freedom	1.58				

\* Estimated standard deviation are in parentheses (1 $\sigma$ ).

*IS*, isomer shift relative to metallic iron absorber; *QS*, quadrupole splitting; *FWHH*, full width at half height.

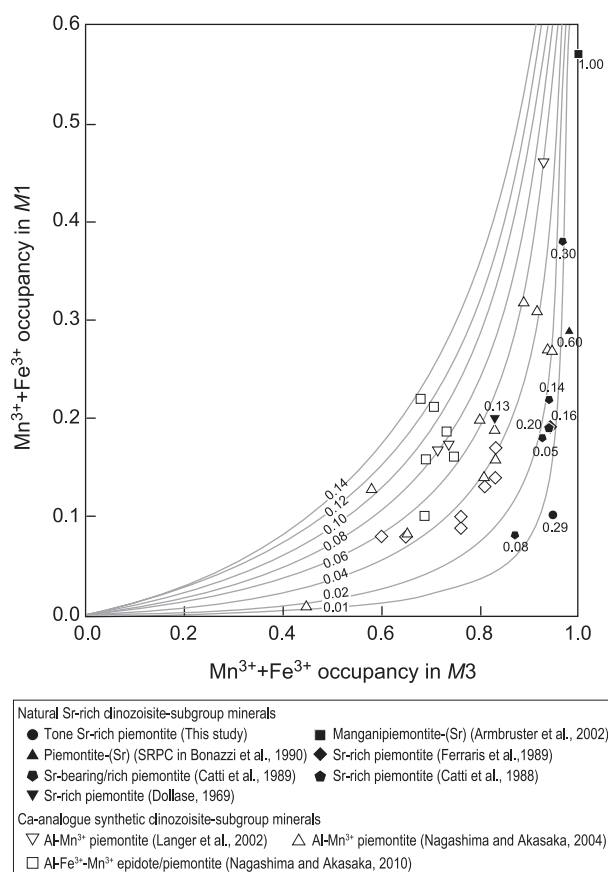


**Figure 5.**  $\text{Mn}^{3+} + \text{Fe}^{3+}$  occupancy at the  $M1$  site versus  $\text{Mn}^{3+} + \text{Fe}^{3+}$  occupancy at the  $M3$  site with intracrystalline partitioning,  $K_D = \frac{[M1(\text{Mn}^{3+} + \text{Fe}^{3+})/M1\text{Al}]}{[M3(\text{Mn}^{3+} + \text{Fe}^{3+})/M3\text{Al}]}$ . Ideal fractionation  $K_D$  of 0.01, 0.02, 0.04, 0.08, 0.10, 0.12, and 0.14 are shown. Numbers written with closed symbols are Sr content (apfu).

Akasaka (2004). It means the  $\text{Mn}^{3+}$  distribution between the  $M3$  and  $M1$  sites is not influenced by the ionic substitution of Sr for Ca at the  $A2$  site. Therefore, the stronger preference of  $(\text{Mn}^{3+} + \text{Fe}^{3+})$  for the  $M3$  site in the Tone piemontite is not due to the  $\text{Mn}^{3+}$  distribution in the  $M3$  site but due to the selective distribution of  $\text{Fe}^{3+}$  in the  $M3$  site. Such strong preferential incorporation of  $\text{Fe}^{3+}$  in the  $M3$  site in strontian piemontite has been also recognized in the St. Marcel strontian piemontite analyzed using the single-crystal neutron diffraction method by Ferraris et al. (1989): the  $M3$  and  $M1$  site populations,  $M3[0.61\text{Mn}^{3+} + 0.33\text{Fe}^{3+} + 0.06\text{Al}]$  and  $M1[0.17\text{Mn}^{3+} + 0.02\text{Fe}^{3+} + 0.81\text{Al}]$ , give  $\text{Fe}^{3+}$ -Al partition coefficient between the  $M1$  and  $M3$  sites of  $K_D = 0.005$ , where  $K_D = (\text{Fe}^{3+}/\text{Al})^{M1}/(\text{Fe}^{3+}/\text{Al})^{M3}$ . In synthetic Sr-free Ca-epidotes, a preference of  $\text{Fe}^{3+}$  at the  $M3$  and  $M1$  sites is similar to that of  $\text{Mn}^{3+}$ : the  $K_D$  values of  $\text{Fe}^{3+}$ -Al partitioning in the synthetic  $\text{Ca}_2(\text{Al},\text{Fe}^{3+})_3\text{Si}_3\text{O}_{12}(\text{OH})$ -epidotes are 0.033 to 0.054 (Giuli et al., 1999), and those in the synthetic  $\text{Ca}_2(\text{Al}_2\text{Fe}_{1.0-0.75}\text{Mn}_{0.0-0.25})\text{Si}_3\text{O}_{12}(\text{OH})$ -epidotes are 0.055-0.063 (Nagashima and Akasaka, 2010). At first glance, these results seem to indicate that the

substitution of Sr for Ca at the  $A2$  site affect the distribution of  $\text{Fe}^{3+}$  in the  $M3$  and  $M1$  sites. However, Dollase (1973) showed that  $K_D$  values of  $\text{Fe}^{3+}$ -Al partitioning in natural epidotes are  $\sim 0.01$ - $0.02$ , and that epidotes with  $\text{Fe}^{3+} \leq 0.63$  apfu in the  $M3$  site have no detectable  $\text{Fe}^{3+}$  in the  $M1$  site. Fehr and Heuss-Abichler (1997) also got  $K_D$  values of  $\text{Fe}^{3+}$ -Al partitioning, 0.012-0.022, for annealed natural epidotes and supported the result by Dollase (1973). Since the  $\text{Fe}^{3+}$  in the  $M3$  site is 0.316 apfu for the Tone piemontite single crystal and 0.267 apfu in average for the piemontite powder sample, the  $\text{Fe}^{3+}$  distribution only in the  $M3$  site but not in the  $M1$  site in the Tone piemontite is consistent with the result for the natural epidotes after Dollase (1973) and Fehr and Heuss-Abichler (1997). There is no topological reason for the stronger preference of  $\text{Fe}^{3+}$  than  $\text{Mn}^{3+}$  to the  $M3$  site.

After all, in the Tone piemontite, Al,  $\text{Mn}^{3+}$  and  $\text{Fe}^{3+}$  occupancies in the  $M1$  and  $M3$  sites are not affected by Sr content. In their study on the synthetic epidote and piemontite with the compositions of  $\text{Ca}_2\text{Al}_2(\text{Fe}^{3+},\text{Mn}^{3+})\text{Si}_3\text{O}_{12}(\text{OH})$ , Nagashima and Akasaka (2010) found a rule that  $\text{Fe}^{3+}$  and  $\text{Mn}^{3+}$  distribute among octahedral sites according to their individual distribution schemes by the substitutions of  $\text{Fe}^{3+} \leftrightarrow \text{Al}$  and  $\text{Mn}^{3+} \leftrightarrow \text{Al}$ , respectively. This rule is valid not only for Ca-epidote and Ca-piemontite but also for Sr-rich and -bearing ones.

No dependence of  $\text{Mn}^{3+}$  and  $\text{Fe}^{3+}$  contents in the  $M1$  and  $M3$  sites against Sr content can be also confirmed in terms of the relationship between Sr content and mean  $\langle M3-O \rangle$  and  $\langle M1-O \rangle$  distances, as discussed below. As shown in Table 8, mean  $\langle M3-O \rangle$  and  $\langle M1-O \rangle$  distances of the Tone piemontite,  $\langle M3-O \rangle = 2.050 \text{ \AA}$  and  $\langle M1-O \rangle = 1.923 \text{ \AA}$ , are similar to those of synthetic Ca-piemontite,  $\langle M3-O \rangle = 2.047$ - $2.063 \text{ \AA}$  and  $\langle M1-O \rangle = 1.926$ - $1.956 \text{ \AA}$  after Langer et al. (2002), Almen (1987) and Nagashima and Akasaka (2004, 2010), and of Sr-rich and -bearing piemontites,  $\langle M3-O \rangle = 2.057$ - $2.077 \text{ \AA}$  and  $\langle M1-O \rangle = 1.929$ - $1.946 \text{ \AA}$  (Ferraris et al., 1989; Bonazzi et al., 1990; Nagashima et al., 2010). Therefore, there is no systematic variations of the bond distances and volumes of the  $M3\text{O}_6$  and  $M1\text{O}_6$  octahedra against Sr content at the  $A2$  site for these piemontites. This conclusion is well illustrated in Figure 6a, in which  $\langle M3-O \rangle$  and  $\langle M1-O \rangle$  distances listed in Table 8 are plotted against Sr content in the  $A2$  site. The  $\langle M1-O \rangle$  distance of a tweddillite from Kalahari, South Africa, in which the  $A2$  site is fulfilled with Sr, is  $1.969 \text{ \AA}$  (Armbruster et al., 2002) and, thus, is greater than those of other strontian piemontite and Sr-free Ca-piemontite. However, since the  $(\text{Mn} + \text{Fe})$  content in the  $M1$  site of the Kalahari tweddillite attains 0.57 apfu, Armbruster et al. (2002) explained that the large mean  $\langle M1-O \rangle$  distance is due to

**Table 8.** Site populations in the *A*2, *M*1, and *M*3 sites, ( $Mn^{3+} + Fe^{3+}$ )-content in the octahedral sites and selected bond distances of the synthetic Ca-piemontites and natural Sr-rich piemontites

	Synthetic piemontites*1 (Langer et al., 2002; Almen, 1987)		Synthetic piemontite*1 (Nagashima and Akasaka, 2004)		Synthetic piemontite*1 (Nagashima and Akasaka, 2010)		Sr-bearing piemontite (Dollase, 1969)	Sr-rich piemontite (Ferraris et al., 1989)	Sr-REE-rich piemontite (Nagashima et al., 2010)	Tone Sr-rich piemontite (This study)	Strontioptic montite (Bonazzi et al., 1990)	Tweedillite (Armbruster et al., 2002)
	MK-35/8	PF-66/14	MK-42/1	PM81	Run No.	30						
Sr in <i>A</i> 2 (apfu)	-	-	-	-	-	-	0.13	0.16	0.19	0.289	0.73	1.00
REE in <i>A</i> 2 (apfu)	-	-	-	-	-	-	-	-	0.10	-	-	-
$Me^{3+}$ in <i>M</i> 1+ <i>M</i> 3 (apfu)												
$Mn^{3+}$	0.83	0.98	1.39	1.03	0.73	0.73	0.72	0.78	0.72	0.735	0.86	1.360-1.577*3
$Fe^{3+}$	-	-	-	-	0.12	0.12	0.31	0.35	0.45	0.316	0.32	0.278-0.191*3
$Mn^{3+} + Fe^{3+}$	-	-	-	-	0.85	0.85	1.03	1.13	1.17	1.051	1.18	1.58*4
Refinement method												
<i>A</i> 1- <i>O</i> 7	n.g.*2	n.g.	2.296(2)	2.32(2)	2.272(9)	2.272(9)	2.288(6)	2.281(7)	2.253(5)	2.285(2)	2.227(13)	2.260(7)
<i>A</i> 2- <i>O</i> 2 ( $\times$ 2)	n.g.	n.g.	2.669(2)	2.68(1)	2.726(6)	2.726(6)	2.711(4)	2.737(3)	2.683(3)	2.753(1)	2.715(8)	2.757(4)
<i>O</i> 2' ( $\times$ 2)	n.g.	n.g.	2.534(3)	2.52(1)	2.554(7)	2.554(7)	2.548(4)	2.553(3)	2.557(3)	2.562(1)	2.614(8)	2.663(4)
<i>O</i> 3 ( $\times$ 2)	n.g.	n.g.	2.832(2)	2.74(1)	2.709(6)	2.709(6)	2.745(4)	2.716(3)	2.800(4)	2.686(1)	2.722(9)	2.757(4)
<i>O</i> 7	n.g.	n.g.	2.254(4)	2.24(2)	2.268(9)	2.268(9)	2.277(6)	2.283(7)	2.300(5)	2.303(2)	2.374(12)	2.405(6)
<i>O</i> 10	n.g.	n.g.	2.489(3)	2.55(1)	2.542(8)	2.542(8)	2.541(7)	2.566(6)	2.565(5)	2.592(2)	2.608(10)	2.657(6)
$\langle^{VIII}A2-O\rangle$	2.587	2.598	2.602	2.58	2.60	2.60	2.603	2.608	2.618	2.612	2.636	2.677
<i>A</i> 2- <i>O</i> 8 ( $\times$ 2)	n.g.	n.g.	3.079(1)	3.04(1)	3.027(3)	3.027(3)	3.03	3.031(1)	2.999(2)	3.0180(6)	3.019(4)	3.044(2)
$\langle^XA2-O\rangle$	-	-	2.689	2.68	2.684	2.684	2.69	2.692	2.694	2.693	2.712	2.750
$\langle M1-O\rangle$	1.926	1.927	1.956	1.95	1.935	1.935	1.933	1.932	1.946	1.923	1.929	1.969
$\langle M3-O\rangle$	2.047	2.047	2.063	2.07	2.049	2.049	2.062	2.057	2.077	2.050	2.061	2.068

\*1 Synthesis conditions: MK-35/8, 1.5 GPa and 800°C; PF-66/14, 1.82 GPa and 820°C; MK-42/1, 1.5 GPa and 750°C; PM81, 0.35 GPa and 500°C; Run No. 30, 0.37 GPa and 500°C.

\*2 n.g., not given in the original paper.

\*3 EMPA data. \*4 X-ray structural refinement result.

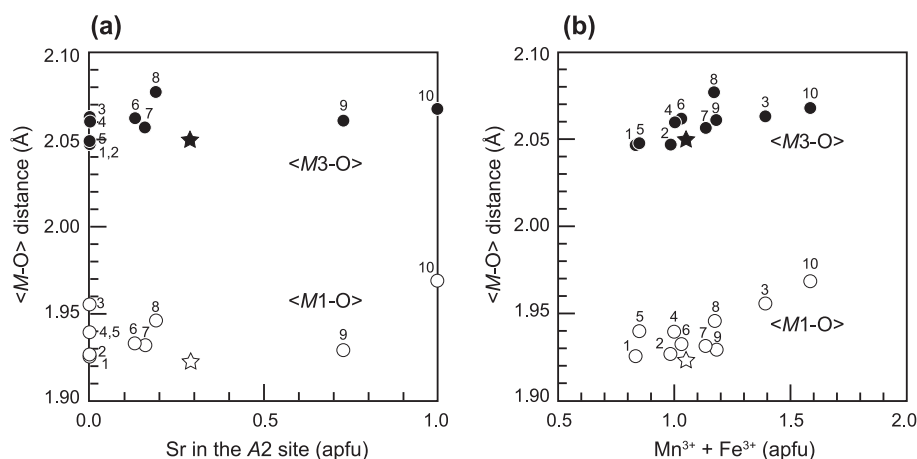


**Figure 6.** Variation of the <M-O> distance as a function of Sr content in the *A2* site (apfu) (a) and Mn<sup>3+</sup> + Fe<sup>3+</sup> content (apfu) (b).

the high (Mn + Fe) content in this site. It is noted that the mean <M3-O> distance, 2.068 Å, of the Kalahari tweddillite is not the largest among the piemontites referred to above, despite the *M3* site fully occupied with (Mn + Fe). Figure 6b shows that the <M3-O> and <M1-O> distances essentially depend on the Mn<sup>3+</sup> and Fe<sup>3+</sup> contents in the *M3* and *M1* sites and supports above discussion and conclusion.

#### Effect of substitution of Sr for Ca in the *A2* site on the *A2O*<sub>10</sub> polyhedra and overall crystal structure

The increase of the mean <*A2*-O> distance with Sr content in the *A2* site is a characteristic geometric change of the *A2O*<sub>10</sub> polyhedron by the Sr substitution for Ca (e.g., Bonazzi and Menchetti, 2004; Nagashima et al., 2010). As shown in Table 8 and Figure 7, the relationships of the <<sup>viii</sup>*A2*-O> (= 2.617 Å) and <<sup>x</sup>*A2*-O> (= 2.693 Å) against Sr content in the *A2* site (= 0.289 apfu) are in harmony with those of other Sr-bearing piemontites. However, it has been found that the *A2O*<sub>8</sub> and *A2O*<sub>10</sub> coordination polyhedra do not expand isotropically with the increase of the Sr content in the *A2* site (Bonazzi et al., 1990; Nagashima et al., 2010): Bonazzi et al. (1990) found main lengthening of the *A2*-O7 distance with Sr in the *A2* site; in addition, Nagashima et al. (2010) found that the *A2*-O2' and *A2*-O10 distances also increase with increasing Sr population in the *A2* site. In fact, the *A2*-O7 distance (= 2.303 Å) of the Tone piemontite with 0.289 apfu Sr is longer than *A2*-O7 = 2.254(4)–2.268(9) Å of the synthetic Sr-free Ca-piemontites (Almen, 1987; Nagashima and Akasaka, 2004, 2010) and close to *A2*-O7 = 2.300(5) Å of the Kamisugai piemontite with Sr = 0.19 apfu (Nagashima et al., 2010). The lengthening of the *A2*-O2' and *A2*-O10 distances by the substitution of Sr for Ca in the *A2* site is also the case of the Tone piemontite: *A2*-O2' = 2.562(1) and *A2*-O10 = 2.592(2) Å of the Tone

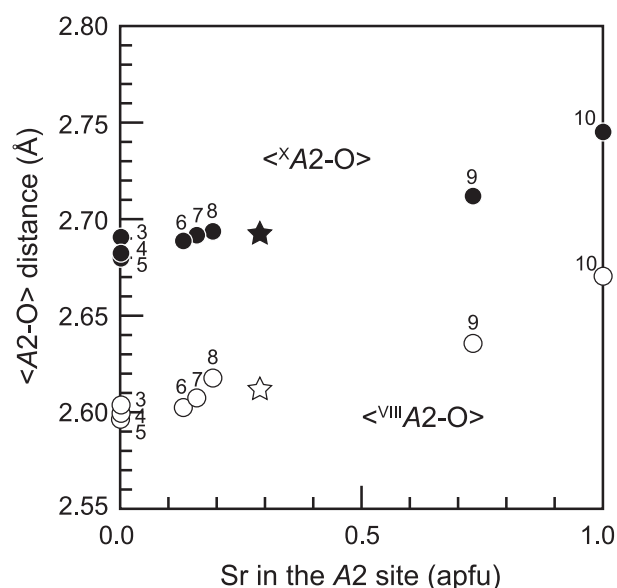


**Figure 7.** Variation of the <*A2*-O> distance as a function of Sr content in the *A2* site (apfu).

piemontite are longer than *A2*-O2' = 2.52(1)–2.554(7) and *A2*-O10 = 2.489(3)–2.55(1) Å of Sr-free Ca-piemontite after Almen (1987) and Nagashima and Akasaka (2004, 2010). The *A2*-O2, *A2*-O3 and *A2*-O8 distances do not show any systematic variation against Sr content, as noted by Nagashima et al. (2010).

Although Bonazzi and Menchetti (2004) noticed that the increase of the *A2*-O7 distance leads to the decrease of the *A1*-O7 distance, the *A1*-O7 distance of the Tone piemontite, 2.285(2) Å, is in a range of those of synthetic Sr-free Ca-piemontites, 2.272(9)–2.296(2) Å (Table 8; Almen, 1987; Nagashima and Akasaka, 2004, 2010). Moreover, as shown in Table 8, the *A1*-O7 distance of the published Sr-bearing or Sr-rich piemontites is in a range between 2.227(13) and 2.288(6) Å. Thus, the *A1*-O7 distance does not seem to be influenced by the

increase of the  $A2-O7$  distance due to the substitution of Sr for Ca at the  $A2$  site.

Anisotropic changes in the  $A2O_{10}$  coordination polyhedra due to the substitution of Sr for effect on the overall crystal structure, which is characteristically represented by the change of the unit-cell parameters and Si1-O9-Si2 angle. The increase of unit-cell parameters of synthetic piemontite in the join  $Ca_2Al_2Mn^{3+}Si_3O_{12}(OH)-Sr_2Al_2Mn^{3+}O_{12}(OH)$  and synthetic clinzoisite in the join  $Ca_2Al_3Si_3O_{12}(OH)-Sr_2Al_3Si_3O_{12}(OH)$  with increasing Sr content in the  $A2$  site has been already shown by Akasaka et al. (2000) and Dörsam et al. (2007), respectively. The unit-cell parameters of the Tone piemontite obtained from the X-ray single-crystal analysis ( $^{42}Sr = 0.289$  apfu;  $Mn^{3+} + Fe^{3+} = 1.051$  apfu),  $a = 8.8942(1)$  Å,  $b = 5.6540(1)$  Å,  $c = 10.1928(2)$  Å,  $\beta = 115.100(1)^\circ$ , and  $V = 464.17(2)$  Å<sup>3</sup>, are fairly consistent with those of the synthetic  $(Ca_{2.0-1.0}Sr_{0.0-1.0})Al_2Mn^{3+}Si_3O_{12}(OH)$ -piemontite reported by Akasaka et al. (2000) [ $a = 8.839(3)-8.94(1)$  Å,  $b = 5.664(2)-5.679(8)$  Å,  $c = 10.166(4)-10.250(7)$  Å,  $\beta = 115.61(3)-115.08(2)^\circ$ , and  $V = 459.0(4)-470(1)$  Å<sup>3</sup>]. Since those of a synthetic Sr-free Ca-piemontite with  $Mn^{3+} = 0.98$  apfu (PF-66/14 after Langer et al., 2002) are  $a = 8.844(1)$  Å,  $b = 5.677(1)$  Å,  $c = 10.167(1)$  Å,  $\beta = 115.54(1)^\circ$  and  $V = 460.6$  Å<sup>3</sup>, the  $a$ - and  $c$ -dimensions and cell volume of our studied piemontite are characteristically greater than those of Sr-free Ca-piemontite. Their similar  $Mn^{3+}$  content allows us to evaluate the pure influence of Sr content because the Jahn-Teller effect is equally applied. The  $\beta$  angle of the Tone piemontite is less than that of the Sr-free Ca-piemontite as well as the published data for Sr-bearing and rich piemontite from other localities (e.g.,  $\beta = 115.40^\circ$  (Dollase, 1969);  $114.71^\circ$  (Nagashima et al., 2010);  $114.54^\circ$  (Bonazzi et al., 1990);  $114.88^\circ$  (Armbruster et al., 2002) and consistent with the suggestion by Dörsam et al. (2007) that the  $\beta$  angle decreases with increasing Sr content.

It has been also noted that the ionic substitution in the  $A$  and  $M$  sites effects not only on the bond lengths and site distortion at each site but also on the geometric connections of the coordination polyhedra, which can be recognized by variation of the bridging angle (e.g., Bonazzi et al., 1992; Bermanec et al., 1994; Armbruster et al., 2002; Nagashima et al., 2010). Dörsam et al. (2007) pointed out that the bridging angle Si1-O9-Si2 increases with the Sr content. In fact, the Si1-O9-Si2 angle of the Tone piemontite,  $155.3^\circ$ , is larger than  $142.9(11)^\circ$  of synthetic PM-81 Ca-piemontite ( $Mn^{3+} = 1.1$ ) after Nagashima and Akasaka (2004) and  $150.6(5)^\circ$  of Run No. 30 Ca-piemontite with  $0.73Mn^{3+} + 0.12Fe^{3+}$  after Nagashima and Akasaka (2010). Therefore, even though the substitution of Sr for Ca at the  $A2$  site does not directly effect on other coordination polyhedra at the  $A1$ , octahe-

dral and tetrahedral sites, it causes the anisotropic change in the  $A2O_8$ - and  $A2O_{10}$ -coordination polyhedra and the Si1-O9-Si2 angle and influences the overall crystal structure of piemontite, which is reflected in the variation of the unit-cell parameters.

## ACKNOWLEDGMENTS

We thank the Editor Dr. T. Kuribayashi, as well as two anonymous reviewers for their constructive comments. Neutron diffraction experiment was performed under proposal No. 2015A0034 in J-PARC. We thank Dr. T. Hattori of J-PARC for his support in the TOF neutron diffraction experiments and Mr. Y. Morifuku for his technical assistance in using EMPA. This work was supported by JSPS KAKENHI Grant Number JP18K03782 to M.N.

## REFERENCES

- Akasaka, M., Sakakibara, M. and Togari, K. (1988) Piemontite from the manganiferous hematite ore deposits in the Tokoro Belt, Hokkaido, Japan. *Mineralogy and Petrology*, 38, 105-116.
- Akasaka, M. and Shinno, I. (1992) Mössbauer spectroscopy and its recent application to silicate mineralogy. *Journal of Mineralogical Society of Japan*, 21, 3-20 (In Japanese with English abstract).
- Akasaka, M., Zheng, Y. and Suzuki, Y. (2000) Maximum strontium content of piemontite formed by hydrothermal synthesis. *Journal of Mineralogical and Petrological Sciences*, 95, 84-94.
- Almen, H. (1987) Kristallchemie von Piemontiten, Änderung der Klinzoisitstruktur durch Einbau von dreiwertigem Mangan. Diplomarbeit, Intitute für Mineralogie und Krietallstrukturlehre, Universität Würzburg, Germany.
- Armbruster, T., Gnos, E., Dixon, R., Gutzmer, J., et al. (2002) Manganvesuvianite and tweddillite, two new  $Mn^{3+}$ -silicate minerals from the Kalahari manganese fields, South Africa. *Mineralogical Magazine*, 66, 137-150.
- Baur, H. (1974) The geometry of polyhedral distortions. Predictive relationships for the phosphate group. *Acta Crystallographica*, B30, 1195-1215.
- Bermanec, V., Armbruster, T. and Oberhansli, R. (1994) Crystal chemistry of Pb- and REE-rich piemontite from Nezilovo, Macedonia. *Schweizerische mineralogische und petrographische Mitteilungen*, 74, 321-328.
- Bonazzi, P., Menchetti, S. and Palenzona, A. (1990) Strontioepiemontite, a new member of the epidote group from Val Graveglia, Liguria, Italy. *European Journal of Mineralogy*, 2, 519-523.
- Bonazzi, P., Garbarino, C. and Menchetti, S. (1992) Crystal chemistry of piemontites: REE-bearing piemontite from Monte Brugiana, Alpi Apuane, Italy. *European Journal of Mineralogy*, 4, 23-33.
- Bonazzi, P. and Menchetti, S. (2004) Manganese in monoclinic members of the epidote group: piemontite and related minerals. In *Epidotes* (Liebscher, A. and Franz, G. Eds.). *Reviews in Mineralogy and Geochemistry*, 56, Mineralogical Society of America and Geochemical Society, Washington, D.C., 495-552.

- Bruker (1999) SMART and SAINT-Plus. Versions 6.01. Bruker AXS Inc., Madison, Wisconsin, USA.
- Catti, M., Ferraris, G. and Ivaldi, G. (1988) Thermal behavior of the crystal structure of strontian piemontite. *American Mineralogist*, 73, 1370-1376.
- Catti, M., Ferraris, G. and Ivaldi, G. (1989) On the crystal chemistry of strontian piemontite with some remarks on the nomenclature of the epidote group. *Neues Jahrbuch für Mineralogie Monatshefte*, 1989, 357-366.
- Dollase, W.A. (1969) Crystal structure and cation ordering of piemontite. *American Mineralogist*, 54, 710-717.
- Dollase, W.A. (1973) Mössbauer spectra and iron distribution in the epidote-group minerals. *Zeitschrift für Kristallographie*, 138, 41-63.
- Dollase, W.A. (1986) Correction of intensities for preferred orientation in powder diffractometry: Application of the March model. *Journal of Applied Crystallography*, 19, 267-272.
- Dörsam, G., Liebscher, A., Wunder, B., Framz, G. and Gottschalk, M. (2007) Crystal chemistry of synthetic  $\text{Ca}_2\text{Al}_3\text{Si}_3\text{O}_{12}\text{OH}$ - $\text{Sr}_2\text{Al}_3\text{Si}_3\text{O}_{12}\text{OH}$  solid-solution series of zoisite and clinozoisite. *American Mineralogist*, 92, 1133-1147.
- Enami, M. (1999) CaAl-silicates: An important Sr container in subducted slab. *Journal of Geography (Chigaku Zasshi)*, 108, 177-187 (in Japanese with English abstract).
- Enami, M. and Banno, Y. (2001) Partitioning of Sr between coexisting minerals of the hollandite- and piemontite-groups in a quartz-rich schist from the Sanbagawa metamorphic belt, Japan. *American Mineralogist*, 86, 205-214.
- Fehr, K.T. and Heuss-Aßbichler, S. (1997) Intracrystalline equilibria and immiscibility along the join clinozoisite-epidote: An experimental and  $^{57}\text{Fe}$  Mössbauer study. *Neues Jahrbuch für Mineralogie Abhandlungen*, 172, 43-67.
- Ferraris, G., Ivaldi, G., Fuess, H. and Gregson, D. (1989) Manganese/iron distribution in a strontian piemontite by neutron diffraction. *Zeitschrift für Kristallographie*, 187, 145-151.
- Franks, F. (1973) *Water: A comprehensive treatise*. vol. 2. pp. 684, Plenum Press, New York.
- Fukushima, H., Minakawa, T. and Nishio, D. (2003) Strontiomelane, barianstroitiopiemontite and hennomartinite from the regional metamorphic manganese ore deposits in the outer zone of Southwest Japan. 203, Abstract of Annual Meeting of Mineralogical Society of Japan (in Japanese).
- Giuli, G., Bonazzi, P. and Menchetti, S. (1999) Al-Fe disorder in synthetic epidotes: A single-crystal X-ray diffraction study. *American Mineralogist*, 84, 933-936.
- Grapes, R. and Watanabe, T. (1984) Al- $\text{Fe}^{3+}$  and Ca- $\text{Sr}^{2+}$  epidotes in metagreywacke-quartzfeldspathic schist, Southern Alps, New Zealand. *American Mineralogist*, 69, 490-498.
- Hattori, T., Sano-Furukawa, A., Arima, H., Komatsu, K., et al. (2015) Design and performance of high-pressure PLANET beamline at pulsed neutron source at J-PARC. *Nuclear Instruments and Methods in Physics Research A*, 780, 55-67.
- Hill, R.J. and Flack, H.D. (1987) The use of the Durbin-Watson  $d$  statistic in Rietveld analysis. *Journal of Applied Crystallography*, 20, 356-361.
- Izumi F. (1993) Rietveld analysis program RIETAN and PREMOS and special applications. In *The Rietveld Method* (Young, R.A. Ed.). pp. 298, Oxford Science Publications, Oxford, UK, 236-253.
- Izumi, F. and Ikeda, T. (2000) A Rietveld analysis program RIETAN-98 and its application to zeolites. *Material Science Forum*, 321-324.
- Izumi, F. and Momma, K. (2007) Three-dimensional visualization in powder diffraction. *Solid State Phenomena*, 130, 15-20.
- Kato, A. and Matsubara, S. (1986) Strontian piemontite. 1986 Joint Annual Meeting (The Japanese Association of Mineralogy, Petrology and Economic Geology, Mineralogical Society of Japan and Society of Resource Geology), 69 (in Japanese).
- Langer, K., Tillmanns, E., Kersten, M., Almen, H. and Arni, R.K. (2002) The crystal chemistry of  $\text{Mn}^{3+}$  in the clino- and ortho-zoisite structure types,  $\text{Ca}_2\text{Mn}_3^{3+}(\text{OH}/\text{O}/\text{SiO}_4/\text{Si}_2\text{O}_7)$ : A structural and spectroscopic study of some natural piemontites and "thulites" and their synthetic equivalents. *Zeitschrift für Kristallographie*, 217, 563-580.
- Liebscher, A. (2004) Spectroscopy of epidote minerals. In *Epidotes* (Liebscher, A. and Franz, G. Eds). pp. 628, Reviews in Mineralogy and Geochemistry, 56, Mineralogical Society of America and Geochemical Society, Washington, D.C., 125-170.
- Mills, S.J., Hatert, F., Nickel, E.H. and Ferraris, G. (2009) The standardisation of mineral group hierarchies: application to recent nomenclature proposals. *European Journal of Mineralogy*, 21, 1073-1080.
- Minakawa, T. (1992) Study on characteristic mineral assemblages and formation process of metamorphosed manganese ore deposits in the Sanbagawa belt. *Memoirs of the Faculty of Science, Ehime University*, 1, 1-74 (in Japanese with English abstract).
- Minakawa, T., Fukushima, H., Nishio-Hamane, D. and Miura, H. (2008) Epidote-(Sr),  $\text{CaSrAl}_2\text{Fe}^{3+}(\text{Si}_2\text{O}_7)(\text{SiO}_4)\text{O}(\text{OH})$ , a new mineral from the Ananai mine, Kochi Prefecture, Japan. *Journal of Mineralogical and Petrological Sciences*, 103, 400-406.
- Miyajima, H., Matsubara, S., Miyawaki, R. and Hirokawa, K. (2003) Niigataite,  $\text{CaSrAl}_3(\text{Si}_2\text{O}_7)(\text{SiO}_4)\text{O}(\text{OH})$ : Sr-analogue of clinozoisite, a member of the epidote group from the Itoigawa-Ohmi district, Niigata Prefecture, central Japan. *Journal of Mineralogical and Petrological Sciences*, 98, 118-129.
- Momma, K. and Izumi, F. (2011) VESTA 3 for three-dimensional visualization of crystal, volumetric and morphology data. *Journal of Applied Crystallography*, 44, 1272-1276.
- Mottana, A. (1986) Blueschist-facies metamorphism of manganeseiferous cherts: A review of the Alpine occurrences. In *Blueschists and Eclogites* (Bernard, W. and Brown, E.H. Eds.). Geological Society of America Memoir, 164, 267-299.
- Nagasaki, A. and Enami, M. (1998) Sr-bearing zoisite and epidote in ultra-high pressure (UHP) metamorphic rocks from the Sulu province, eastern China: An important Sr reservoir under UHP conditions. *American Mineralogist*, 83, 240-247.
- Nagashima, M. and Akasaka, M. (2004) An X-ray Rietveld study of piemontite on the join  $\text{Ca}_2\text{Al}_3\text{Si}_3\text{O}_{12}(\text{OH})$ - $\text{Ca}_2\text{Mn}_3^{3+}\text{Si}_3\text{O}_{12}(\text{OH})$  formed by hydrothermal synthesis. *American Mineralogist*, 89, 1119-1129.
- Nagashima, M., Akasaka, M. and Sakurai, T. (2006) Chromian epidote in omphacite rocks from the Sanbagawa metamorphic belt, central Shikoku, Japan. *Journal of Mineralogical and Petrological Sciences*, 101, 157-169.
- Nagashima, M., Akasaka, M., Kyono, A., Makino, K. and Ikeda, K. (2007) Distribution of chromium among the octahedral sites in chromian epidote from Iratsu, central Shikoku, Japan. *Journal of Mineralogical and Petrological Sciences*, 102, 240-254.
- Nagashima, M. and Akasaka, M. (2010) X-ray Rietveld and  $^{57}\text{Fe}$  Mössbauer studies of epidote and piemontite on the join  $\text{Ca}_2\text{Al}_3\text{Si}_3\text{O}_{12}(\text{OH})$ - $\text{Ca}_2\text{Al}_2\text{Fe}^{3+}\text{Si}_3\text{O}_{12}(\text{OH})$ - $\text{Ca}_2\text{Al}_2\text{Mn}^{3+}\text{Si}_3\text{O}_{12}(\text{OH})$  formed by hydrothermal synthesis. *American Mineralo-*

- gist, 95, 1237-1246.
- Nagashima, M., Armbruster, T., Akasaka, M. and Minakawa, T. (2010) Crystal chemistry of Mn<sup>2+</sup>-, Sr-rich and REE-bearing piemontite from the Kamisugai mine in the Sambagawa metamorphic belt, Shikoku, Japan. *Journal of Mineralogical and Petrological Sciences*, 105, 142-150.
- Nishiyama, T. (1990) CO<sub>2</sub>-metasomatism of a metabasite block in a serpentinite mélange from the Nishisonogi metamorphic rocks, southwest Japan. *Contributions to Mineralogy and Petrology*, 104, 35-46.
- Oishi, R., Yonemura, M., Nishimaki, Y., Torii, S., et al. (2009) Rietveld analysis software for J-PARC. *Nuclear Instruments and Methods in Physics Research A* 600: 94-96.
- Oishi-Tomiyasu, R., Yonemura, M. and Morishima, T. (2012) Application of matrix decomposition algorithms for singular matrices to the Pawley method in *Z-Rietveld*. *Journal of Applied Crystallography*, 45, 299-308.
- Perseil, E.A. (1990) Sur la présence du strontium dans les minéralisations manganésidère de Falotta et de Parsettens (Grisons-Suisse)-evolution des parageneses. *Schweizerische Mineralogische und Petrographische Mitteilungen*, 70, 315-320.
- Raudsepp, M., Hawthorne, F.C. and Turnock, A.C. (1990) Evaluation of the Rietveld method for the characterization of fine-grained products of mineral synthesis: the diopside-hedenbergite join. *Canadian Mineralogist*, 28, 93-109.
- Reinecke, T. (1986) Crystal chemistry and reactions of piemontites and thulites from highly oxidized low grade metamorphic rocks at Vitali, Andros Island, Greece. *Contributions to Mineralogy and Petrology*, 93, 56-76.
- Robinson, K., Gibbs, G.V. and Ribbe, P.H. (1971) Quadratic elongation: a quantitative measure of distortion in coordination polyhedra. *Science*, 172, 567-570.
- Sheldrick, G.M. (1996) SADABS. University of Göttingen, Germany.
- Sheldrick, G.M. (2015) Crystal structure refinement with SHELX. *Acta Crystallographica*, C71, 3-8.
- Togari, K., Akasaka, M., Sakakibara, M. and Watanabe, T. (1988) Mineralogy of manganese iron ore deposits and chert from the Tokoro Belt, Hokkaido. *Mining Geology Special Issue*, 12, 115-126.
- Torres-Ruiz, J., Pesquera, A. and Sanchez-Vizcaino, V. (2003) Chromian tourmaline and associated Cr-bearing minerals from the Nevado-Filábride Complex (Betic Cordilleras, SE Spain). *Mineralogical Magazine*, 67, 517-533.
- Treloar, P. (1987) Chromian muscovites and epidotes from Outokumpu, Finland. *Mineralogical Magazine*, 51, 593-599.
- Whitney, D.L. and Evans, B.W. (2010) Abbreviations of names of rock-forming minerals. *American Mineralogist*, 95, 185-187.
- Yoshimura, T. (1952) Manganese deposits of Japan. pp. 567, *Mangan-Kenkyukai* (in Japanese).
- Young, R.A. (1993) Introduction to the Rietveld method. In *The Rietveld Method* (Young, R.A. Ed.). pp. 298, Oxford Science Publications, Oxford, UK, 1-38.

*Manuscript received November 22, 2019*

*Manuscript accepted June 21, 2020*

*Published online October 8, 2020*

*Manuscript handled by Takahiro Kuribayashi*